



## LJMU Research Online

**Kadhim, A, Sadique, MM, Al-Mufti, R and Hashim, KS**

**Developing One-Part Alkali-Activated metakaolin/natural pozzolan Binders using Lime Waste as activation Agent**

<http://researchonline.ljmu.ac.uk/id/eprint/13619/>

### Article

**Citation** (please note it is advisable to refer to the publisher's version if you intend to cite from this work)

**Kadhim, A, Sadique, MM, Al-Mufti, R and Hashim, KS (2020) Developing One-Part Alkali-Activated metakaolin/natural pozzolan Binders using Lime Waste as activation Agent. Advances in Cement Research. ISSN 0951-7197**

LJMU has developed [LJMU Research Online](#) for users to access the research output of the University more effectively. Copyright © and Moral Rights for the papers on this site are retained by the individual authors and/or other copyright owners. Users may download and/or print one copy of any article(s) in LJMU Research Online to facilitate their private study or for non-commercial research. You may not engage in further distribution of the material or use it for any profit-making activities or any commercial gain.

The version presented here may differ from the published version or from the version of the record. Please see the repository URL above for details on accessing the published version and note that access may require a subscription.

For more information please contact [researchonline@ljmu.ac.uk](mailto:researchonline@ljmu.ac.uk)

<http://researchonline.ljmu.ac.uk/>

# Developing One-Part Alkali-Activated metakaolin/natural pozzolan Binders using Lime Waste as activation Agent

\*Abdullah Kadhim<sup>a, b</sup> ([a.m.kadhim@2017.ljmu.ac.uk](mailto:a.m.kadhim@2017.ljmu.ac.uk)), Monower Sadique<sup>a</sup> ([M.M.Sadique@ljmu.ac.uk](mailto:M.M.Sadique@ljmu.ac.uk)), Rafal Al-Mufti<sup>a</sup> ([R.A.LatifAlMufti@ljmu.ac.uk](mailto:R.A.LatifAlMufti@ljmu.ac.uk)), Khalid Hashim<sup>a</sup> ([K.S.Hashim@ljmu.ac.uk](mailto:K.S.Hashim@ljmu.ac.uk)),

(a) Department of Civil Engineering, Liverpool John Moores University, Henry Cotton Building, Webster Street, Liverpool L3 2ET, UK.

(b) Department of Civil Engineering, College of Engineering, University of Babylon, Babylon, Iraq.

## Abstract

Among the several schemes that have been reported to be a satisfactory alternative to Portland cement is Alkali Activated Cement (AAC), which has recently started to gain greater consideration in construction sectors. Conventional two-part alkali activation has many drawbacks, including the activating solution being viscous, problematic and non-user friendly to handle. Thus, this research aims to produce a one-part alkali activated metakaolin/natural pozzolan, by using an earth alkaline source (rich in CaO) from waste material (lime kiln dust), as an activating precursor to break the alumina-silicate crystalline phases. Thermal treatment of materials at two levels of treatment (450°C and 950°C), was used as an assisted activation approach. Analytical techniques including X-Ray powder diffraction XRD, Thermogravimetric Analysis TG-DTA, Fourier Transform Infrared Spectroscopy FTIR and Scanning Electron Microscope SEM, were utilised to investigate the performance of the developed materials at a molecular level. Reduction of crystalline peaks as well as the appearance of new wollastonite minerals within the calcined lime kiln dust, contributed to the development of 27 MPa compressive strength after 28 days. The dissolution made through the pozzolanic reaction as well as thermal treatment evidently contributed to transform crystalline to amorphous phases.

## Keywords

Alkali-activated cements , Lime, Thermal behaviour, , Diffraction (X-ray, neutron, electron), Thermal analysis, Infrared (R, FTIR).

## 33 1. Introduction

34 The world production of the Ordinary Portland Cement (OPC) is growing and reached 4.1 billion  
35 metric tonnes in 2018(U.S. Geological Survey, 2019). The use of Portland cement in concrete  
36 construction is under serious evaluation, because of substantial challenges that are facing the  
37 method of production for conventional cement. Firstly, the energy consumption through the whole  
38 process. Secondly, the high quantity of carbon dioxide gas (CO<sub>2</sub>) is released to the atmosphere  
39 through the production of cement (Demie *et al.*, 2013). Alternatively, there are noteworthy  
40 investigations to develop other types of cements that are entirely free of (OPC) and based  
41 principally on green raw materials. Mineral Products Association (MPA) in the UK, listed a  
42 number of novel (non-Portland) cements with low energy in their fact sheet (Mineralproducts.org,  
43 2017). One of these novel cements is Alkali Activated Cement (AAC). AACs are cementitious  
44 materials, formed as a result of an alkaline reaction with amorphous or vitreous alumina-silicates.  
45 When mixed with alkaline activators (solid or liquids) in a chemical reaction called alkali-  
46 activation or alkalination, these materials set and harden, yielding a material with good binding  
47 properties (Davidovits, 1993; Provis, 2017). Conventional two-part alkali activation (wherein a  
48 solid raw material is activated with alkaline chemical solution) has many drawbacks: the hazardous  
49 activating solution, which makes it non-user friendly to handle. On the other hand, the activator  
50 solutions of alumina-silicate material represents a real concern through the use of (AAC). The  
51 activator solutions provide the highest single contribution to the embodied carbon dioxide of  
52 (AAC) (Van Deventer *et al.*, 2012; Provis *et al.*, 2015; Luukkonen *et al.*, 2018). Until now, it  
53 cannot be said that (AAC) are based on friendly and environmentally friendly process, as the  
54 production of the chemical solutions releases large amounts of CO<sub>2</sub> to the environment (Torres-  
55 Carrasco *et al.*, 2017).

56 Several efforts have been made to develop a one-part alkali activated cement (AAC) which can be  
57 found under different terminology in the literature, such as one-part alkali activated cement, self-  
58 activating cement or one-part alkali alumina-silicate hydraulic cement (Matakah *et al.*, 2016;  
59 Almalkawi *et al.*, 2017; Ban *et al.*, 2017). In one-part mixtures, only a dry mixture is needed in  
60 addition to water. The dry mixture is prepared by mixing a solid alkali-activator with a solid  
61 alumina-silicate precursor, with or without an assisted activation approach (Matakah *et al.*, 2016;  
62 Luukkonen *et al.*, 2018; Abdel-Gawwad *et al.*, 2019).

63 Provis (2014), defined the activators as any substance that represents an alkaline source that raises  
64 the pH of the reaction mixture and simplifies dissolution. This includes alkali cations (Na<sup>+</sup>, K<sup>+</sup>) or  
65 earth alkaline cations (Ca<sup>+2</sup>, Mg<sup>+2</sup>). A substantial number of published studies that explored the  
66 synthesis of one-part (AAC), have used alkaline commercial solid chemical activators, including  
67 primarily sodium hydroxide (NaOH) aided by other chemical agents to improve the alkalination  
68 in binder such as sodium silicates (Na<sub>2</sub>SiO<sub>3</sub>), sodium carbonates (Na<sub>2</sub>CO<sub>3</sub>). Realistic reports  
69 revealed that these chemicals are expensive and primarily contribute to the total cost of production  
70 of (AAC) cost (Weerd, 2011; Van Deventer *et al.*, 2012; Heath *et al.*, 2013; Kim *et al.*, 2013).

71 Therefore, using solid chemicals do not represent a realistic commercial or environmental optimal  
72 solution that can be used as an activator (Luukkonen *et al.*, 2018).

73 Previous studies have reported on the use of (CaO) and Ca(OH)<sub>2</sub> as potential alternative activators,  
74 as these activators are cheaper than (NaOH or Na<sub>2</sub>SiO<sub>3</sub>) (Kim *et al.*, 2013; Vaccari *et al.*, 2013).  
75 For instance, the total cost of NaOH is nearly 5-6 times higher than that CaO global (Vaccari *et al.*,  
76 2013) These activators provide alkaline earth cations in place of alkali cations, which ease the  
77 creation of different binding phases, when compared to blends of low calcium content (Li *et al.*,  
78 2010; Luukkonen *et al.*, 2018). An earlier study by Cabrera and Rojas (2001) investigated the  
79 metakaolin-lime-water system by thermal analysis. The study confirmed the appearance of  
80 reaction products encompassing principally Strätlingite (C<sub>2</sub>ASH<sub>8</sub>) and tetra calcium aluminium  
81 hydrate (C<sub>4</sub>AH<sub>13</sub>) as the reason for binder strength development. Kim *et al.* (2013), used  
82 commercial (CaO) solid powder to produce non-cement binder, with ground granulated blast  
83 furnace slag as the Si/Al source material. When compared to Ca(OH)<sub>2</sub>, CaO activator was noticed  
84 to provide a higher mechanical strength up to 53 MPa at 56 days due to the production of more  
85 (C-S-H) than Ca(OH)<sub>2</sub>. Nevertheless, when investigating the energy and ecological analysis of  
86 synthesising high purity chemical CaO powder, it was discovered that the synthesis process has  
87 high energy consumptions and a complicated process requiring a high level of accuracy(Licht,  
88 2016)('Production of purified calcium carbonate', 1993). Different activation assisted methods  
89 were used in the production of one-part (AAC). Thermal activation (calcination) was used recently  
90 as an assisted approach to improve the reactivity and the amorphicity of supplementary  
91 cementitious materials, such as natural pozzolans (Almalkawi *et al.*, 2017; Abdel-Gawwad and  
92 Khalil, 2018). During the thermal treatment of material, crystalline bonds are broken down and  
93 transformed to a glassy or amorphous phase resulting in a more reactive binder.

94 The principal aim of this work is the development of novel approach to produce a one-part (AAC)  
95 without the need to the presence of commercial chemical activator. This will be achieved by  
96 providing the earth alkaline source from a by-product waste material, which is primarily composed  
97 of reactive (CaO). This by-product results from the production of quick lime known as lime kiln  
98 dust (LKD), which is regularly disposed of in landfills worldwide. For instance, in the USA, it is  
99 estimated that about 2.5 million metric tonnes of high-calcium LKD is produced annually(Miller  
100 *et al.*, 2004). Thus, LKD requires reuse, in order to lessen environmental problems and promote  
101 sustainability. LKD is mainly composed of a CaO compound and high alkaline materials (high  
102 pH). Presence of reactive CaO in material with high quantities contributes to raise the alkalinity  
103 scale (PH) in which is leading to high level of dissolutions. This was proved by past studies that  
104 used materials of CaO to enhance the reactivity of binder matrix such (Kim *et al.*, 2013; Vaccari  
105 *et al.*, 2013). Other studies used even OPC as a source for CaO to improve the properties of their  
106 developed products such Nath and Sarker (2015).

107 A combination of metakaolin, which is the crystallographically disordered layered product of  
108 dihydroxylation of kaolinite (an alumina-silicate clay) (Rashad, 2013; Provis *et al.*, 2014) and  
109 volcanic tuff or natural pozzolan were used as an alumina silicate (Al/Si) source to formulate one-  
110 part dry AAC powder that just needs water to produce the binding material. Volcanic tuffs, provide

111 an extensive variety of reactivity, dependent upon their degree of crystallinity and mineralogy. The  
 112 proposed Alumina-silicate precursors, undertake dissolution and precipitation processes when  
 113 mixed with lime or CaO, yielding calcium alumina-silicate hydrate (C-A-S-H) (Nath *et al.*, 2015).  
 114 As for the traditional method (with alkaline chemicals) of producing AAC, in addition to the  
 115 related health and safety concerns which increase the production cost, there is a limited production  
 116 capacity of these chemicals as they need high accuracy and huge plants. For instance, sodium  
 117 hydroxide (NaOH) is currently produced at approximate rate 60 Mt per year via the chlor-alkali  
 118 process and up-scaling this production is not straightforward because chlorine (Cl<sub>2</sub>), which has a  
 119 limited world-market, is produced as a side-product (Provis, 2017; Luukkonen *et al.*, 2018).  
 120 Therefore, replacing synthetic alkali silicates with other alkali and silica sources is important.  
 121 Hence, this study represents an attempt and evaluation of the performance of one-part (AAC)  
 122 comprised from a combination of (Al/Si) activated by waste material rich of (CaO). Thermal  
 123 treatment was used as an assisted activation method to increase the reactivity and amorphicity of  
 124 raw materials. Materials were characterised in terms of their physical, chemical, metallurgical and  
 125 thermogravimetric properties to reveal the changes after thermal treatment.

## 126 2. Materials and methods

### 127 2.1 Materials used

128 The proposed materials were collected from various suppliers in the UK to ensure their local  
 129 availability . The alumina-silicate source was produced by combination of metakaolin (MK) and  
 130 a volcanic tuff or natural pozzolan (NP) which were supplied by two commercial suppliers. For  
 131 improved alkalinity within the blended system, lime kiln dust (LKD) was used that was also  
 132 supplied by a waste producing industry in the UK. The proposed materials were assessed and  
 133 characterised to evaluate their physico-chemical properties and have been tabulated in Table 1  
 134 below. The specific surface area was determined by air permeability test (Blaine method) which  
 135 is described in BS EN 196-6 (2010).

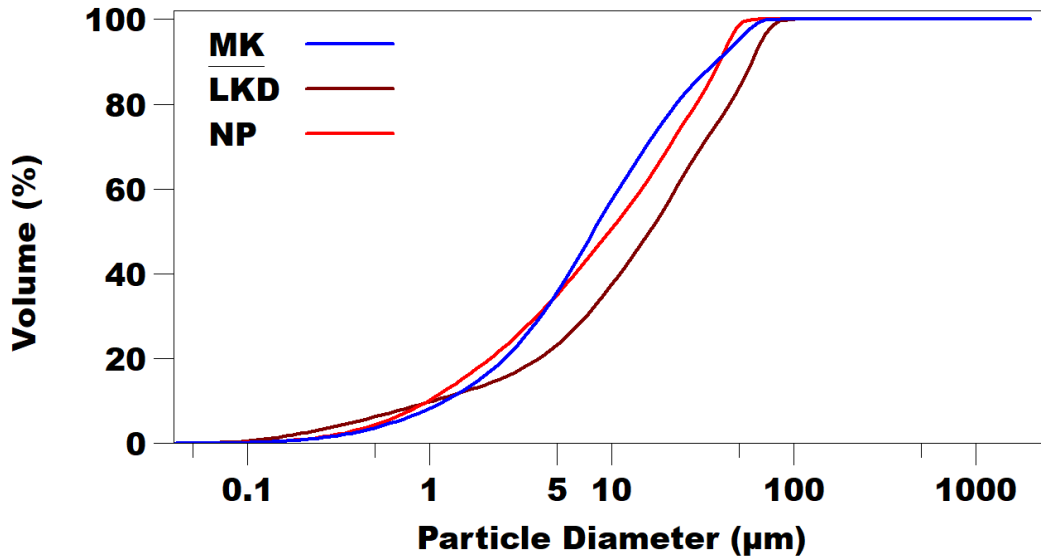
136  
137

*Table 1. Physical properties of undisturbed materials.*

Material	Specific surface area (Blaine) (cm <sup>2</sup> /g)	pH	Density (g/cm <sup>3</sup> )
MK	196000	6	2.69
NP	172000	6	2.57
LKD	101000	12.3	2.7

138  
139  
140

141 Particle size distribution (PSD), was determined by Beckman Coulter laser diffraction particle size  
 142 analyser as shown in Figure. 1. MK and NP were identified as having similar size distributions  
 143 with ( $D_{50}$ ) being 9.22, 7.87 $\mu\text{m}$  respectively. Conversely, LKD was found to be coarser with a ( $D_{50}$ )  
 144 15.94 $\mu\text{m}$ . This particle size range of raw materials has high positive effect on alkali activation  
 145 reaction. Rashad (2016), reported that as the grain size is lower than 32  $\mu\text{m}$  of MK, providing  
 146 workable mix with higher compressive strength.



147  
 148

*Figure 1. Particle size distribution (PSD) of starting materials.*

149 The elemental composition of raw materials was determined, as they were received using a  
 150 Shimadzu EDX 720, energy dispersive X-ray fluorescence (EDXRF) spectrometer. The key oxide  
 151 elements are listed in Table 2. It is shown that MK and NP are mainly composed of  $\text{SiO}_2$  and  $\text{Al}_2\text{O}_3$ ,  
 152 which can be considered as an ideal source of siliceous and aluminate materials, with minor  
 153 quantities of  $\text{CaO}$ ,  $\text{Na}_2\text{O}$ ,  $\text{K}_2\text{O}$  and  $\text{MgO}$  in NP. LKD is mostly rich in  $\text{CaO}$  of 80.1Wt.% with  
 154 slight amounts of  $\text{SiO}_2$  and  $\text{Na}_2\text{O}$ , therefore it was considered as calcareous source.

155  
 156

*Table 2. Chemical composition by XRF of raw materials (Wt.%).*

Components (wt. %)	$\text{SiO}_2$	$\text{Al}_2\text{O}_3$	$\text{Fe}_2\text{O}_3$	$\text{CaO}$	$\text{Na}_2\text{O}$	$\text{K}_2\text{O}$	$\text{MgO}$	$\text{TiO}_2$
<b>MK</b>	55	40	1.4	0.15	0.4	0.4	0.95	1.7
<b>NP</b>	46.6	30.4	3.8	4.5	3.9	6	4.2	0.6
<b>LKD</b>	14.6	0.2	0.1	80.1	3.8	0.5	0.6	0.1

157

## 158 2.2 Characterisation Methods

159 In order to further investigate the behaviour and the performance of the materials and assess their  
160 chemical mineralogy and microstructure, the following characterisation techniques have been  
161 utilised:

### 162 2.2.1 Energy-Dispersive X-ray diffraction (EDXRD)

163 X-ray diffraction (XRD), is the elastic scattering of x-ray photons by atoms in a periodic lattice.  
164 The scattered monochromatic x-rays that are in phase, produce constructive interference  
165 (Ramachandran *et al.*, 2000). XRD was used in this research to determine the amorphous content  
166 and the mineralogy phases of each material. The test was carried out using a Rigaku mini-flex  
167 diffractometer (mini-flex goniometer), with CuK X-ray radiation (30 kV voltage and 15mA current  
168 at scanning speed of 2.0deg./min in continuous scan mode) and scanning range:  $2\theta = 5-65^\circ$ . XRD  
169 was investigated for the raw materials before and after thermal treatment at (950°C and 450°C).  
170 Moreover, a small sample of each (AAC) hydrated and hardened paste were finely grinded, dried,  
171 and at age of 28 days investigated via XRD analysis for mortars with the highest strength.

### 172 2.2.2 Thermogravimetric Analysis (TGA)

173 Thermal analysis, is used to monitor the mass of material as a mean of temperature or time as the  
174 sample specimen is subjected to a controlled temperature program, in a controlled atmosphere.  
175 Thermal analysis used in this investigation, consisted of Thermogravimetric analysis (TG), which  
176 usually determines thermal events related to weight loss of the sample. However, this technique  
177 does not detect phase change, such as “melting”; and differential thermal analysis (DTA) is  
178 employed, which is the first derivative of the weight loss curve. DTA indicates phase changes as  
179 endothermic and exothermic peaks (Hill *et al.*, 2019). Therefore, it is denoted as TG-DTA  
180 technique. The tests were completed using the Perkin Elmer TGA Q50 V20.13 Build 39. The  
181 thermal performance of materials was investigated by TG-DTA, with a heating range 20-900°C  
182 and a heating rate 10 °C/min. In this study, TG-DTA investigations were performed for raw  
183 materials to assess their thermal behaviours during individual calcination.

### 184 2.2.3 Fourier Transform Infrared Spectroscopy (FT-IR)

185 FT-IR, represents a supplementary technique for the assessment of elemental compositions,  
186 chemical bonds and molecular vibrations of samples. Infrared (IR) radiation is distributed over a  
187 sample. In this investigation, FT-IR was conducted for raw materials and for hardened pastes at  
188 age of 28 days for specimens of the highest strength. FT-IR analysis was carried out by using a  
189 Perkin-Elmer Spectrum BX series Fourier transform infrared spectrometer (FT-IR), equipped with  
190 a Miracle ATR accessory (Specac, UK). The spectrum of the sample was recorded by  
191 accumulating 16 scans at  $4\text{cm}^{-1}$  resolution and wavelength between ( $524\text{cm}^{-1}$  and  $2000\text{cm}^{-1}$ ).

#### 192 2.2.4 Scanning Electron Microscope (SEM) & Energy Dispersive X-rays Spectroscopy (EDX)

193 SEM morphological analysis and observations were conducted for raw materials and hardened  
194 pastes at age of 28 days . EDX is an analytical system where element specific radiation is used for  
195 chemical characterisation of the surface near volume. With the aid of proper detectors, the energy  
196 or the X-rays are determined. EDX, when combined with SEM, provides elemental analysis on  
197 areas as small as nano-metres in diameter. In this study, EDX-SEM was conducted using an Oxford  
198 Inca x-act detector (45nA prob current and 100 sec counting time) and a FEI SEM model Inspect  
199 S(20kV accelerating voltage) for hardened pastes at age of 28 days. One day before the 28 days,  
200 pastes were removed from water curing and left to dry in room temperature air (20°C). This step  
201 was conducted in order to avoid coating with gold when performing EDX as this might affect the  
202 spectrum elemental analysis.

#### 203 2.2.5 Compressive strength

204 The compressive strength of mortar prisms, was based as a function for evaluating the mechanical  
205 properties of specimens and was measured according to the standard BS EN 196-1 (2016). The  
206 test was carried out by a Control Automax 5 compression tester, with a load rate of 0.4 MPa/sec.

### 207 2.3 Characterisation of materials

208 The XRD, SEM, FT-IR and TG-DTA analysis of undisturbed materials has been illustrated in  
209 Figures 2 to 5. From the X-Ray diffractions of MK as shown in Figure. 2, it is observable that MK  
210 comprises many crystalline phases and is primarily composed of quartz ( $\text{SiO}_2$ ), and (Mullite  
211  $\text{Al}_6\text{Si}_2\text{O}_{13}$ ) in major crystalline peaks.

212 Kaolinite ( $\text{Al}_2\text{Si}_2\text{O}_5(\text{OH})_4$ ) and Illite ( $(\text{K},\text{H}_3\text{O})(\text{Al},\text{Mg},\text{Fe})_2(\text{Si},\text{Al})_4\text{O}_{10}[(\text{OH})_2,(\text{H}_2\text{O})]$ ) compounds  
213 in minor peaks. Highest quartz peak was at  $(2\theta)$   $26.73^\circ$ . Diffractogram pattern of NP, which has  
214 closely crystalline peaks with the highest quartz peak at  $(2\theta)$   $26^\circ$ . Smaller peaks are formed by  
215 feldspars such as Anorthite ( $\text{CaAl}_2\text{Si}_2\text{O}_8$ ) and Clinoptilolite ( $\text{KNa}_2\text{Ca}_2(\text{SiO}_2)_9\text{Al}_7\text{O}_{72}\cdot 24\text{H}_2\text{O}$ ).  
216 Moreover, Edenite ( $\text{Ca}_2\text{NaMg}_5(\text{AlSi}_7)\text{O}_{22}(\text{OH})_2$ ) was present in NP diffractions with high  
217 quantities. Diffractions of LKD show one recognised crystalline peak of lime (CaO) a with high  
218 intensity. Smaller peaks exist in forms of quartz ( $\text{SiO}_2$ ), Natrosilites ( $\text{Na}_2\text{Si}_2\text{O}_5$ ) and Ertixiite  
219 ( $\text{Na}_2\text{Si}_4\text{O}_9$ ). The presence of such compounds, increases alkalinity activity in LKD, which are  
220 similar to the content of water glass ( $\text{Na}_2\text{SiO}_3$ ) commercial activator.



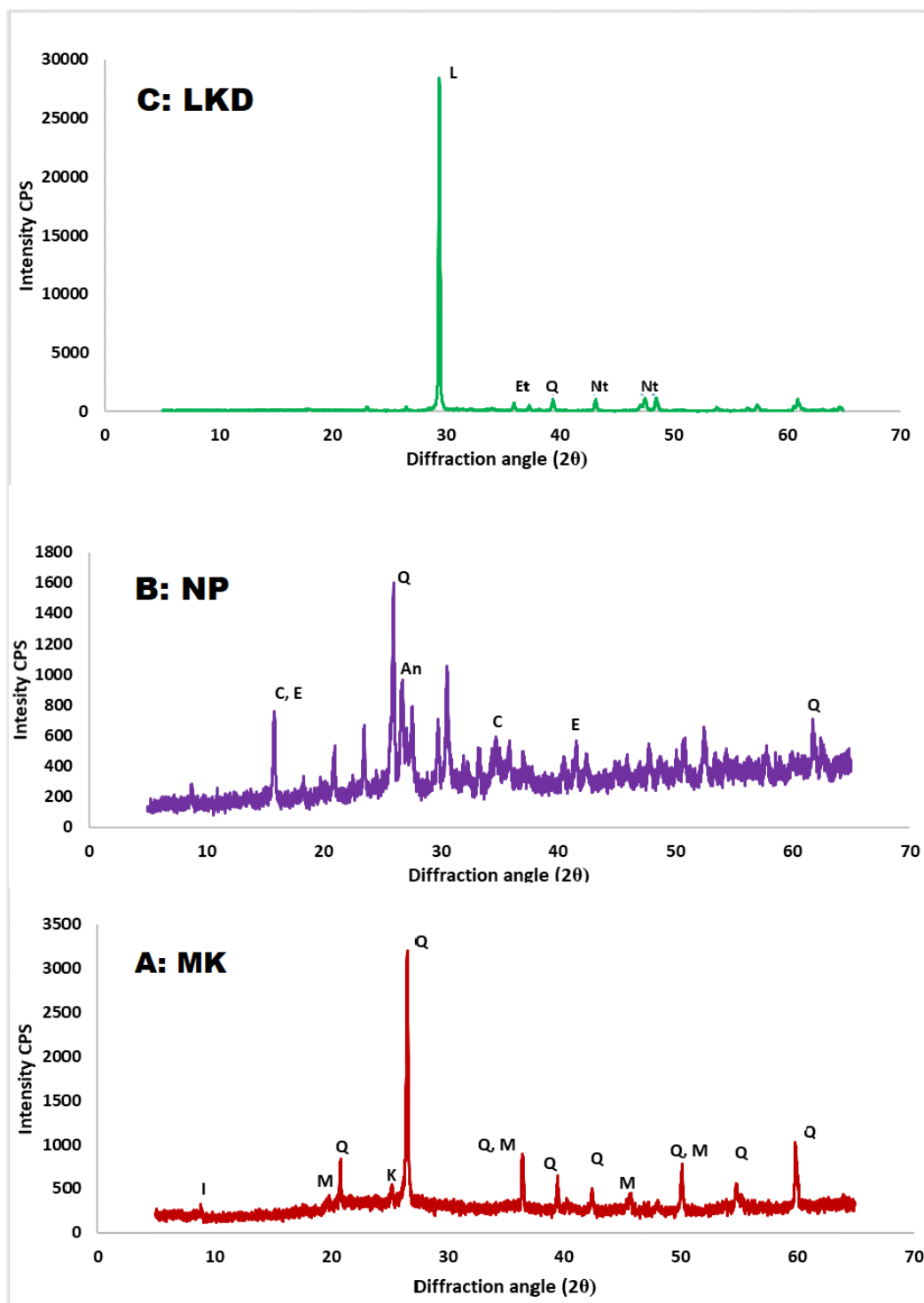


Figure 2. XRD-patterns of initial materials

Q: Quartz, K: kaolinite, M: Mullite, I: Illite, C: Clinoptilolite, An: Anorthite, E: Edenite, L: Lime, Nt : Natrosilites, Et: Ertixiite.

221

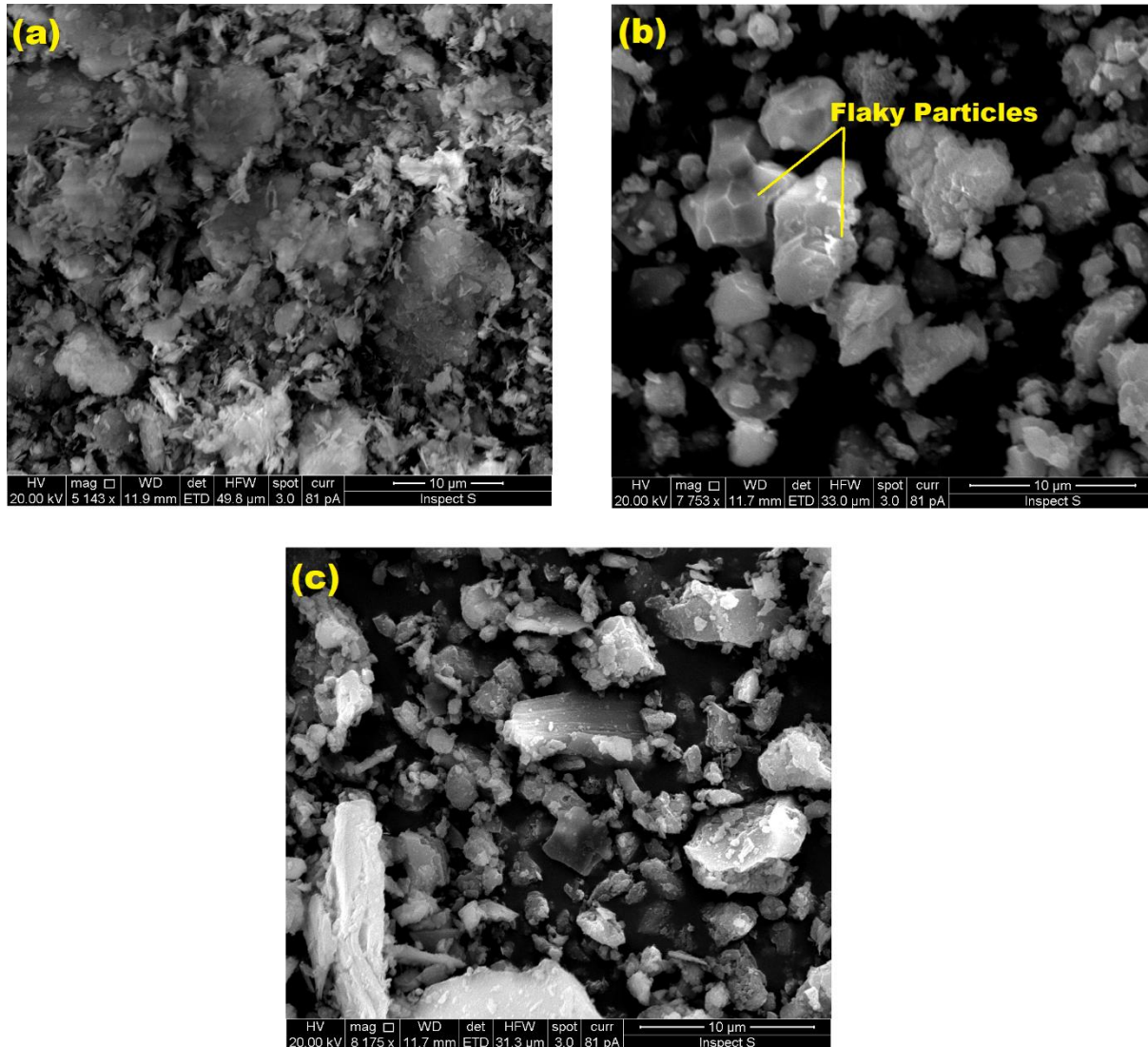
222

223

224

225

226 Scanning electron microscope images illustrating the particles of original materials, as shown in  
227 Figure. 3. MK, seems to have fine and lamellar particles with random non uniform shapes. Particles  
228 of LKD look coarser and have less surface area with flaky shapes. The raw NP particles, as shown  
229 in the SEM image, are irregular in shape and size.

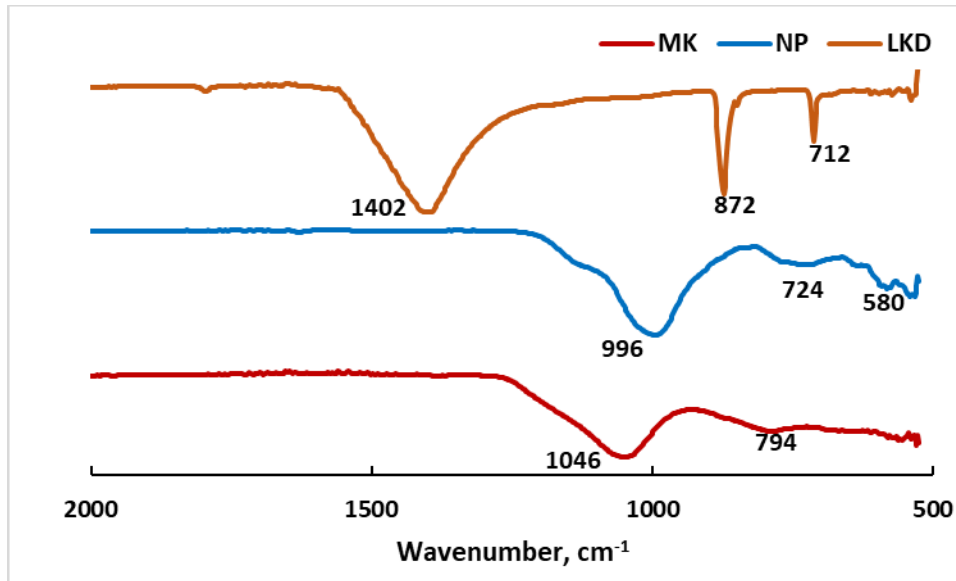


230  
231

Figure 3. SEM micrographs of a) MK, b) LKD and c) NP.

232 In Figure. 4 , FT-IR measurements of raw MK and NP are indicating the that highest absorption  
233 bands at  $1046\text{ cm}^{-1}$  and  $996\text{ cm}^{-1}$  respectively, which were attributed to the strong bands of Si–O–  
234 Al and tetrahedral Si–O–Si of bridging oxygen (BO) atoms of the original alumina-silicate  
235 framework (Vizcayno *et al.*, 2010). The characteristic peaks appearing at  $794\text{ cm}^{-1}$  and  $724\text{ cm}^{-1}$ ,  
236 are ascribed to the stretching vibration Si–O and stretching Al 6-coordinated geometry (AL, Mg)–  
237 O–OH (Nayak *et al.*, 2007). Both absorptions Si–O–Si and Si–O, are supporting the presence of  
238 quartz, while Si–O–Al is supporting the presence of kaolinite (Kakali *et al.*, 2001; Nayak *et al.*,  
239 2007). These peaks are related to the alumina-silicate prevalence phases in both MK and NP. The

240 strong presence of calcite ( $\text{CaCO}_3$ ) presented by the C–O bond, was evidently presented by the  
241 bands at 1402, 872 and 712 $\text{cm}^{-1}$  (Miguel *et al.*, 2009). The presence of these bands are accredited  
242 to the tendency of CaO to react naturally with  $\text{CO}_2$  in the atmosphere.



243  
244 *Figure 4. FTIR-spectra of Raw MK, NP and LKD*

245  
246 Figure. 5A exhibits the thermal performance of NP investigated by TG-DTA, when calcined to  
247 900°C. As can be seen, some mass-loss phases are present in its patterns caused by endothermic  
248 and exothermic reactions. The thermogravimetric (TG) patterns of NP mass-loss from room  
249 temperature to 900°C is approximately 7% of the total weight, which might be attributed to the  
250 loss of chemically and physically adsorbed water and breakdown of crystal phases, which was  
251 evidenced by XRD analysis. The loss of weight can be divided into three stages. The loss from 20-  
252 320°C is due to the evaporation of adsorbed water. The loss from 320 – 620°C, is because of  
253 calcining amounts of impurities and contaminants. While loss from 620 to 900°C is due to  
254 decomposition of unburnt carbons (Duxson *et al.*, 2007; He *et al.*, 2010). As for the DTA curve,  
255 there was endothermic convexity at 119 °C, which relates to the evaporation of water followed by  
256 exothermic concavity at 250°C. The TG curve of MK has shown a very small weight change within  
257 2% of the total weight, with a reasonably straight DTA curve, as shown in Figure. 5B. The TG  
258 patterns of LKD have revealed that it has not lost any weight until 350°C; with there was slight  
259 weight loss. While the peak which starts from 600 °C and ends with 750 °C, the weight changed  
260 dramatically with a 40 % loss of original weight and an exothermic sharp peak of the DTA curve,  
261 which is shown clearly in Figure. 5C. This loss is markedly attributed to the transformation and  
262 loss of the CaO crystalline intense peak, which was further evidenced by the XRD analysis of  
263 950°C calcination, when this peak disappeared from the diffraction pattern.

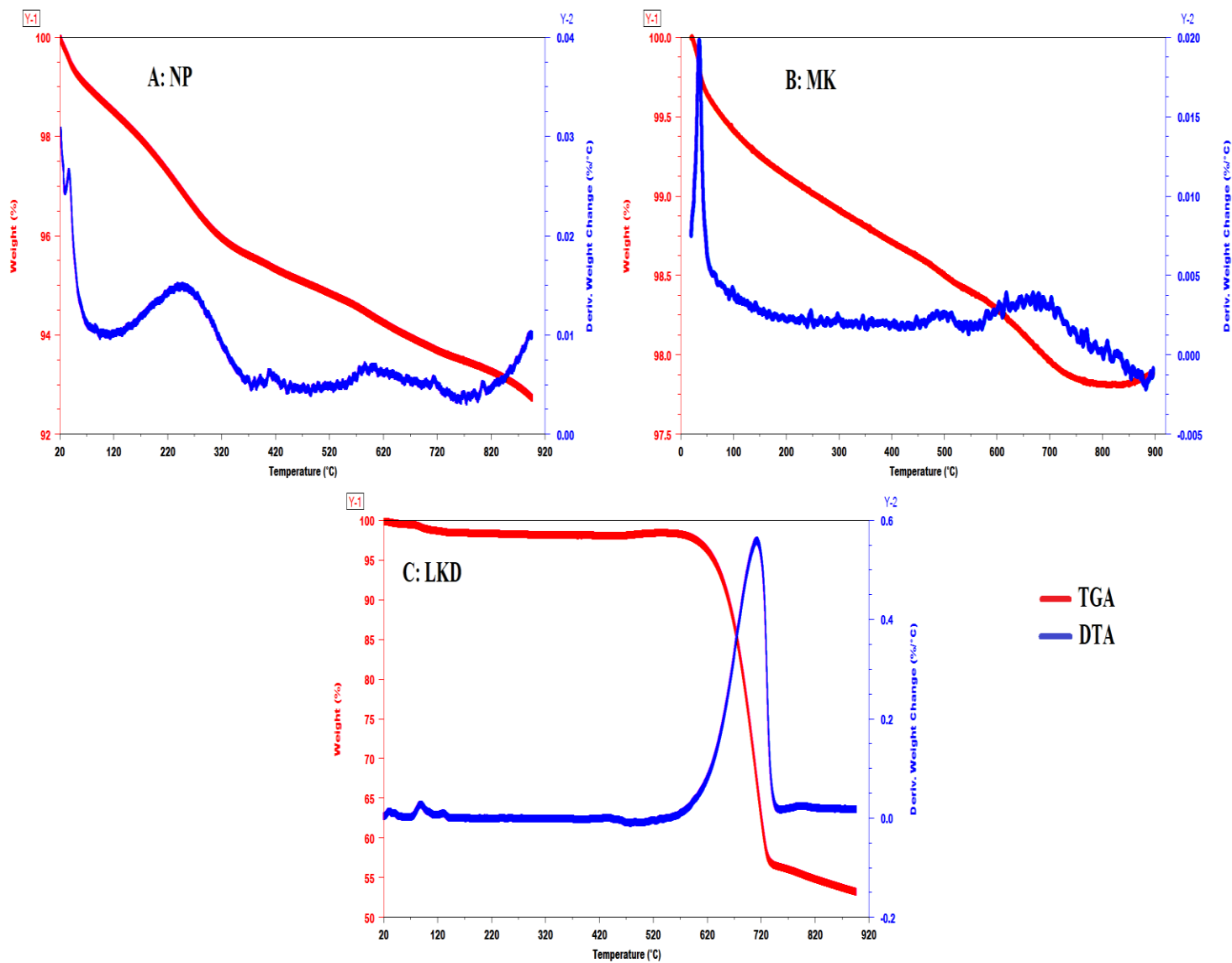


Figure 5. TG-DTA curves of A: NP, B: MK, C: LKD

265  
 266  
 267  
 268  
 269  
 270  
 271

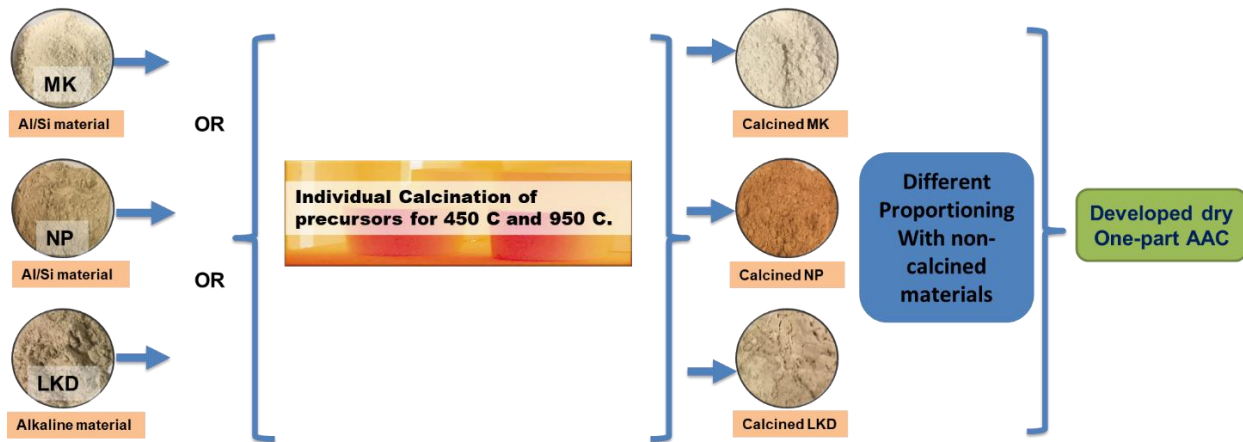
## 272 2.4 Alkaline activated cement (AAC) synthesis

### 273 2.4.1 Thermal activation

274 Thermal treatment or calcination, means heating the substance to high temperature (500-2000<sup>0</sup>C)  
275 within a controlled atmosphere, in order to increase their reactivity by changing their mineralogy.  
276 Thermal treatment is used as one of the assisting activation methods to produce one-part (AAC)  
277 cement. Most of the materials, which are clayey in origin, require calcination in order to be  
278 reactive. For instance, metakaolin (Al<sub>2</sub>Si<sub>2</sub>O<sub>7</sub>) is originally synthesised from the calcination of  
279 kaolin clay (Al<sub>2</sub>SiO<sub>5</sub> (OH)<sub>4</sub>) (Ilić *et al.*, 2010). During the calcination process, dihydroxylation is  
280 carried out, leading to the loss of the long-range order of alumina and silica layers and conversion  
281 of the powder to an amorphous form. Another change is that the alumina transforms from the  
282 octahedral coordination to tetrahedral coordination, due to calcination (Justnes *et al.*, 1990).  
283 Thermal activation was performed for the materials individually to increase their reactivity and to  
284 evaluate the effect of each calcined material on the blended properties. Subsequently, mixing each  
285 calcined material with the other two non-calcined precursors according to the blending concept  
286 (Si/Al+alkaline) was carried out to synthesise a dry hydraulic cement, as illustrated in Figure. 6.  
287 Thermal treatment was conducted in a muffle furnace with a ramping temperature of 20 <sup>0</sup>C/min  
288 for 2 hours. Two foundry cylindrical silicon carbide graphite crucibles (500ml) and two alumina  
289 cylindrical crucibles (175ml), were used during calcination. It was stated from past studies that  
290 crystallinity and reactivity of most materials rich in alumina-silicate content can increase with  
291 temperatures up to 750 -1200<sup>0</sup>C and after this temperature range, their reactivity can be decreased  
292 (Sanz *et al.*, 1988; Yao *et al.*, 2009; Davidovits, 2017; Peng *et al.*, 2017). However, Davidovits  
293 (2017) stated that the intensity line of the most reactive Al species existed in MK, Al(5) and Al(4)  
294 are becoming very well defined at temperature 900 °C for 4 hours calcination time. Therefore, 950  
295 °C for 2hours was used in this study for MK calcination.

296 In this study activation at 450 °C temperature at mid-range between 0 and 950<sup>0</sup>C was also  
297 investigated to evaluate and compare the phase transitions. Noteworthy that during treatment some  
298 of the material colours have changed in both stages of temperatures. MK was becoming whiter as  
299 increasing temperature as shown in Figure. 6. NP has shown considerable changing from greyish  
300 colour to brown as high as temperature. The colour transformation of NP attributed to the  
301 increment of anorthite mineral that been observed clearly in XRD patterns which turned to be  
302 brown in nature(Kimata *et al.*, 1996). LKD originally white but turned with a little greyish at  
303 950<sup>0</sup>C.

304

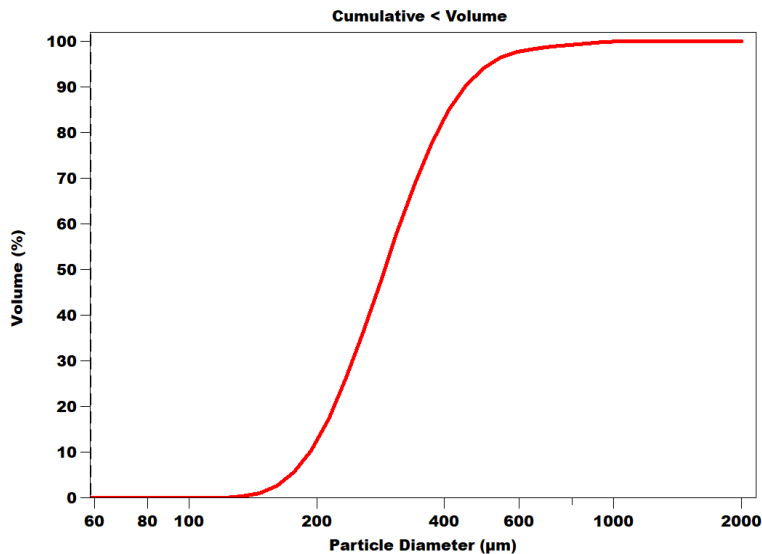


305  
306  
307

Figure 6. Preparation steps of one-part (AAC)

#### 308 2.4.2 Formation of hydraulic cement mortar

309 CEN standard kiln dried sand in accordance with BS EN 196-1 (2016) and supplied from (Tarmac)  
310 was used in mortars with particle size distribution shown in Figure. 7 and a specific gravity of 2.62  
311  $\text{g/cm}^3$  with binder to sand ratio is (1:2). The mixing procedure was followed according to the  
312 requirements of BS EN 196-1 (2016). Initially, 0.55 water/binder ratio was chosen, but it was  
313 found that the mortars were extremely workable therefore; it was reduced to 0.45 for all the  
314 mortars, where appropriate consistency was achieved at this stage.



315  
316

Figure 7 Particle Size Distribution of the used sand

317 Initially, raw materials were mixed before treatment based on their chemical elements to form  
318 (Al/Si) + alkaline system. Based on this, the formulation designs of materials were as shown in  
319 Table 3. Firstly, MK and LKD (50M50L) were mixed with 50% each to evaluate the strength

320 obtained from the combination. Compressive strength was tested on 7, 14 and 28 days of the mixes.  
 321 This step was conducted to find out which materials gathering are making the highest strength.  
 322

Table 3. Initial mixes proportion

Mix ID	Binder contents
50M50L	MK 50% LKD 50%
75M25L	MK 75% LKD 25%
25M75L	MK 25% LKD 75%
25M65M10N	MK 25% LKD 65% NP 10%
40M40L20N	MK 40% LKD 40% NP 20%

323  
 324 However, the compressive strength of these initial mixes as shown in Figure 8 below does not  
 325 show significant strength except (25M75L) which is 20 MPa at age 28 days. The attempt of  
 326 optimising this mix by the inclusion of 10% and 20% of NP as (25M65M10N and 40M40L20N)  
 327 in the above table has caused sharp reduction in strength at this stage as shown in Figure 8.

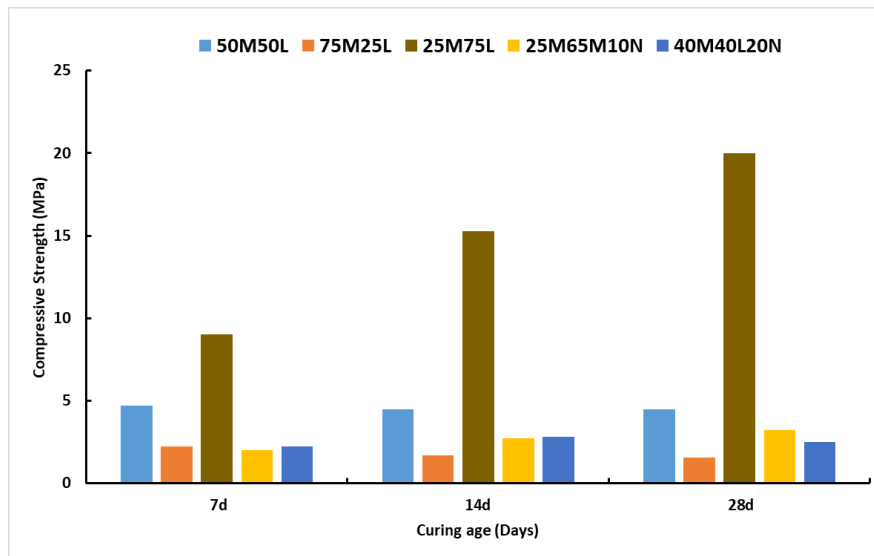


Figure 8. Compressive strength of initial mixes

328  
 329  
 330 The optimum mix from the initial stage with no thermal treatment was mix of (25M75L). This mix  
 331 was investigated for thermal treatment with both of its components have been calcined individually  
 332 but did not provide change of strength compared to the state of no thermal treatment. However,  
 333 the only considerable change was noticed when NP was added of 20% and 30% with calcined  
 334 LKD was reduced to 40% and 30% as illustrated in the results of 40M40(L-950)20N and  
 335 35M35(L-950)30N respectively.

336 The dry one-part AAC powder mixes were blended in ternary process as shown below in Table 4  
 337 with different mix compositions. The dry powder was mixed in mechanical mixer (Hobart 5 litre  
 338 mixer) for 3 minutes to homogenise the mixture. Afterward, the tap water and sand were added  
 339 respectively and the mixing of mortar is carried out to obtain a uniform mortar mixture. The  
 340 blended mortars were casted in steel prism moulds (40 mm × 40 mm × 160 mm). After 24 hour,  
 341 the hardened specimens were demoulded and were cured in a hot water curing regime to enhance  
 342 the reactivity and the hydration rate of the mortars. In mortars activated with alkaline chemicals in  
 343 which mainly consisting of Sodium hydroxide (NaOH), there is high possibility that the produced  
 344 system to suffer problems of efflorescence, micro cracking as a result of dehydration which causes  
 345 decrease in compressive strength (Li *et al.*, 2013). The need for relative humidity is mainly to  
 346 tackle the aforementioned issues with systems made of chemicals as high levels of heat are  
 347 generated as a result of sodium species dissolution which lead to cracks (Peng *et al.*, 2017). In this  
 348 study, hot water is mainly used for accelerating and promoting the hydration reactions during the  
 349 curing period. Curing temperature was fixed to 50 °C for 7 days and then cured in normal 20 °C  
 350 water until 28 days as suggested by Perera (2007) and Singh (2015).

351 *Table 4. Mixing proportions of blends.*

Mix ID	Binder contents	Calcination temperature (°C)	Calcined constituent
40M40L20(N-950)	40%MK 40%LKD 20%NP	950	NP
40(M-950)40L20N	40%MK 40%LKD 20%NP	950	MK
40M40(L-950)20N	40%MK 40%LKD 20%NP	950	LKD
(40M40L20N)-950	40%MK 40%LKD 20%NP	950	NP, MK, LKD
35M35L30(N-950)	35%MK 35%LKD 30%NP	950	NP
35(M-950)35L30N	35%MK 35%LKD 30%NP	950	MK
35M35(L-950)30N	35%MK 35%LKD 30%NP	950	LKD
(35M35L30N)-950	35%MK 35%LKD 30%NP	950	NP, MK, LKD
35M35L30(N-450)	35%MK 35%LKD 30%NP	450	NP
35(M-450)35L30N	35%MK 35%LKD 30%NP	450	MK
35M35(L-450)30N	35%MK 35%LKD 30%NP	450	LKD
(35M35L30N)-450	35%MK 35%LKD 30%NP	450	NP, MK, LKD

352

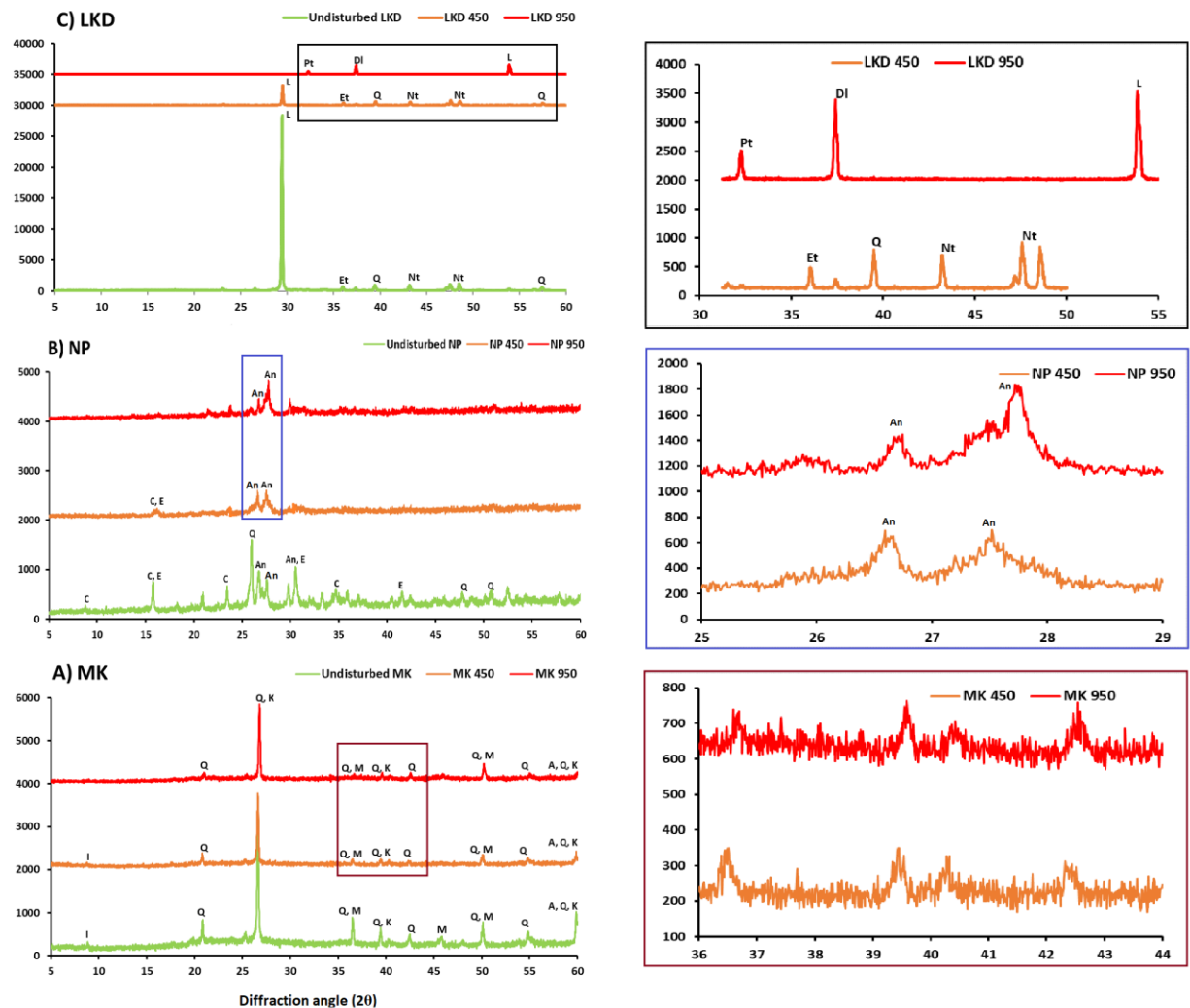


### 353 3. Results and discussion

#### 354 3.1 Effect of thermal treatment on mineralogy

355 The powder diffraction of calcined materials has been shown in Figure. 9. Diffractograms of MK,  
356 have revealed a significant reduction and even disappearance of kaolinite and quartz peaks after  
357 both levels of calcination indicating semi-transformation of material to an amorphous phase.

358 XRD spectrums of calcined NP at both levels, indicated a huge transformation of crystalline  
359 phases to amorphous phases through the loss of quartz and clinoptilolite, in a range of  $2\theta$  from 30  
360  $^{\circ}$  to  $60^{\circ}$ . It can be noticed, that crystalline quartz peak at  $2\theta = 26^{\circ}$  has disappeared entirely when  
361 NP calcined to  $450^{\circ}\text{C}$  and  $950^{\circ}\text{C}$ , introducing strong evidence of the increment of amorphicity.  
362 This was confirmed by the formulation of a broad amorphous hump of anorthite existed at  $2\theta =$   
363  $26.7^{\circ}$  and  $2\theta = 27.8^{\circ}$  at  $950^{\circ}\text{C}$  patterns. Remarkably, this intense peak in LKD was diminished  
364 markedly when calcined to  $450^{\circ}\text{C}$  and completely disappeared in  $950^{\circ}\text{C}$  calcination. The  
365 appearance of new diffraction patterns at new angles of calcined LKD at  $950^{\circ}\text{C}$ , indicated  
366 formation of the new compounds, but was composed of the same elements as untreated LKD  
367 (CaO, SiO<sub>2</sub> and Na<sub>2</sub>O) in the form of wollastonite minerals; dectolite (NaCa<sub>2</sub>Si<sub>3</sub>O<sub>8</sub>(OH)) and  
368 dellaite (Ca<sub>6</sub>Si<sub>3</sub>O<sub>11</sub>(OH)<sub>2</sub>) (Eilers *et al.*, 1983; Garbev *et al.*, 2008). This was accompanied by the  
369 complete disappearance of the intense crystalline CaO at  $950^{\circ}\text{C}$  calcination, which indicated that  
370 calcination had caused a large combination of lime CaO with the compounds of SiO<sub>2</sub> and Na<sub>2</sub>O,  
371 to form the above compounds.



372

373

Figure 9. XRD patterns of materials after thermal treatment A)MK, B)NP, C)LKD.

374

*Q: Quartz, K: kaolinite, M: Mullite, A: Anatas, I: Illite, C: Clinoptilolite, An: Anorthite, E: Edenite, L:*

375

*Lime, Pt: Pectolite, Dl: Dellaite, Nt : Natrosilites, Et: Ertixiite.*

376

### 3.2 Effect of thermal treatment on molecular bonds

377

The FT-IR spectrums of thermally treated materials are illustrated in Figure. 10. The alumina-

378

silicate bands Si-O-Si and Si-O-Al, have been become higher from  $1046\text{cm}^{-1}$  in untreated MK to

379

$1058\text{cm}^{-1}$  at  $450^\circ\text{C}$  and  $1078\text{cm}^{-1}$  at  $950^\circ\text{C}$ . This while the opposite to this tendency took place

380

with the spectra of NP. This kind of shifting and enhancement of broadness of these bands, leads

381

to the transformation of crystalline phases to an amorphous structure and high deformation in the

382

lengths and angles of Si-O-Al and Si-O-Si bonds (Abdel-Gawwad, García, *et al.*, 2018). This

383

transformation is satisfied by the increment of non-bridging oxygen atoms due to thermal treatment

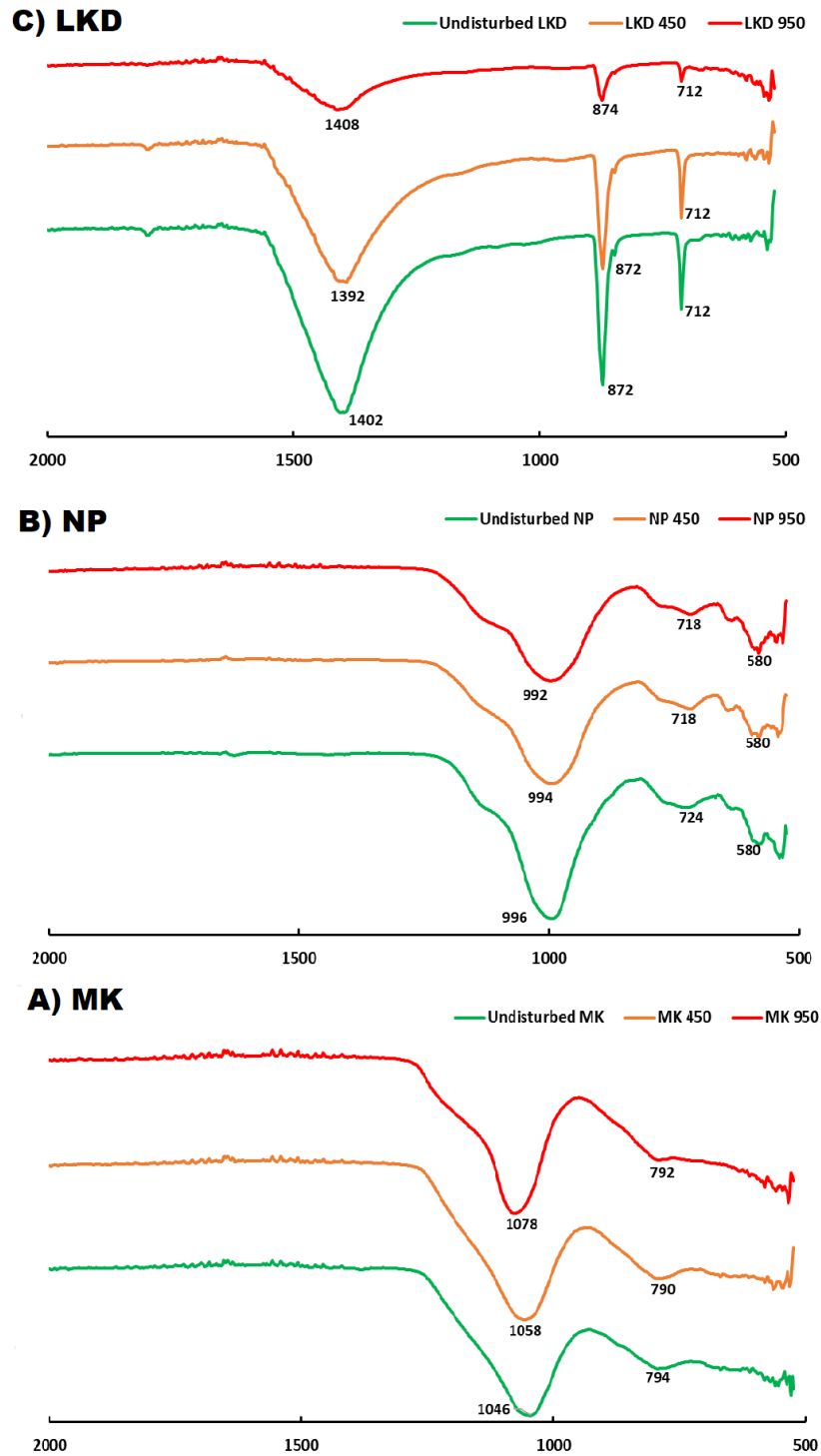
384

(Feng *et al.*, 2012). A considerable shifting of the C-O bond from  $1402\text{cm}^{-1}$  to  $1408\text{cm}^{-1}$  during

385

the treatment at  $950^\circ\text{C}$ , indicates the transformation of the crystalline phase in to the glassy phase.

386 It can be noticed that the C-O band became wider and less intense at 950 °C spectra. The intensity  
387 reduction of this band, interprets the increment of pure CaO amounts released from CaCO<sub>3</sub>.



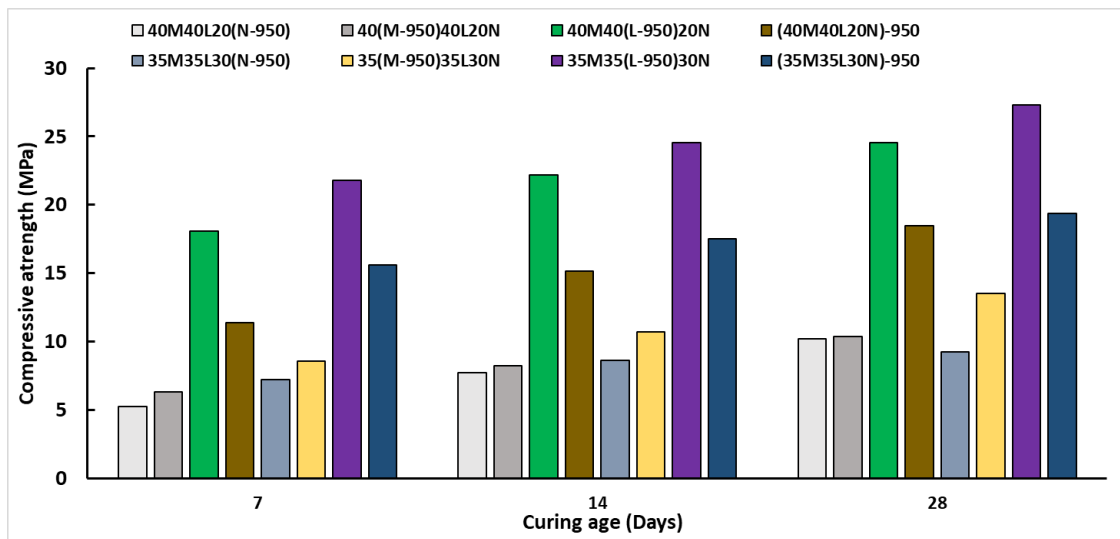
388  
389

Figure 10. FTIR spectra of materials after thermal treatment.

### 390 3.3 Compressive strength

391 After treatment, there was a considerable increase in the compressive strength as indicated in  
 392 Figure. 11. The blend containing only calcined LKD (40M40(L-950)20N) has shown a  
 393 compressive strength of 24.54MPa after 28 days. The regular growth in strength of up-to 28 days  
 394 for this blend indicates that hydration of raw materials was progressive with time. This  
 395 development of the strength of this mix, was due to the calcination of LKD with the presence of  
 396 sufficient amounts of reactive silicate and calcium oxide from the NP. A considerable amount of  
 397 strength was developed within the mix, containing calcined materials individually and collectively,  
 398 which has showed no cementitious properties prior to thermal treatment. Calcination at 950°C,  
 399 clearly contributed to a huge variation in LKD mineralogy and substantial reduction in its  
 400 crystallinity, which was observed in the XRD patterns. In order to optimise the strength, these  
 401 mortar mixes were repeated with the same procedure, but increases the proportion of NP to  
 402 (35%MK 35%LKD 30%NP). The increment of the NP amount, was due to the suitable  
 403 composition of NP, which contains a various range of alkaline elements including CaO, Na<sub>2</sub>O and  
 404 K<sub>2</sub>O, as shown in XRF results. Noticeably, the highest compressive strength was achieved at this  
 405 stage with 27.3MPa in 28 days for (35M35(L-950)30N) , as shown in Figure. 11. The increment  
 406 of NP weight from 20% to 30% in mortars, resulted in the growth of more C-A-S-H products. The  
 407 addition of more NP contributed to extra dissolution of quartz silicate, caused by CaO and Na<sub>2</sub>O  
 408 that exist in the calcined LKD and NP, yielding high binding properties. Therefore, a higher  
 409 transformation to vitreous mineralogy led to a higher strength of (35M35(L-950)30N). Moreover,  
 410 the fall in strength for (35M35L30N)-950) when all three components are calcined, indicated a  
 411 lesser dissolution of Si/Al compounds from MK and NP, which means that less activation was  
 412 caused by LKD.

413



414

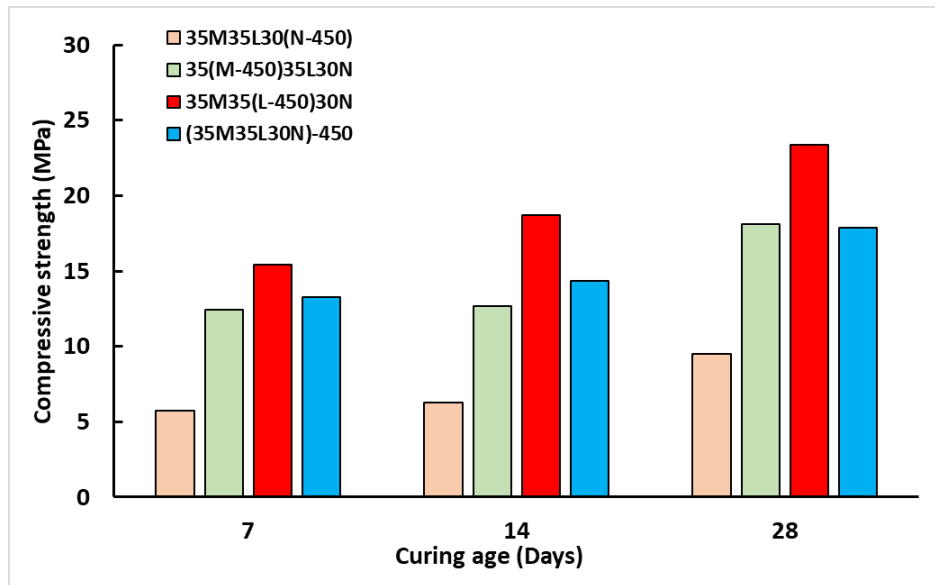
415

Figure 11. Compressive strength after 950 °C calcination.

416

417 The TG-DTA curves have shown that the weight loss of the constituents of this ternary blend,  
418 starts at the temperatures in the range 350-500°C. Furthermore, this was evidenced by XRD  
419 patterns, where raw materials after 450°C treatment have displayed a considerable change in their  
420 diffraction. Therefore, the ternary blend of 35% MK 35% LKD 30% NP was formulated after 450°C  
421 treatment with same process of mixing. The resulting compressive strength offered by the ternary  
422 blends after 450°C treatment, has been shown in Figure. 12. A similar trend of higher strength in  
423 the case of calcining LKD individually at 450°C, was evident in (35M35(L-450)30N) with  
424 23.4MPa at age of 28 days. Although both early and longer-term strength were higher in the case  
425 of high temperature 950°C treatment, no remarkable strength generation was observed compared  
426 to a lower temperature treatment (450°C). This similar development of strength is ascribed to  
427 mineralogical and chemical changes that were noticed in both XRD and DT-TGA results, which  
428 indicated that most of diffraction patterns were starting to transform around 450°C.

429



430

431

Figure 12. Compressive strength after 450°C calcination

432

433

434

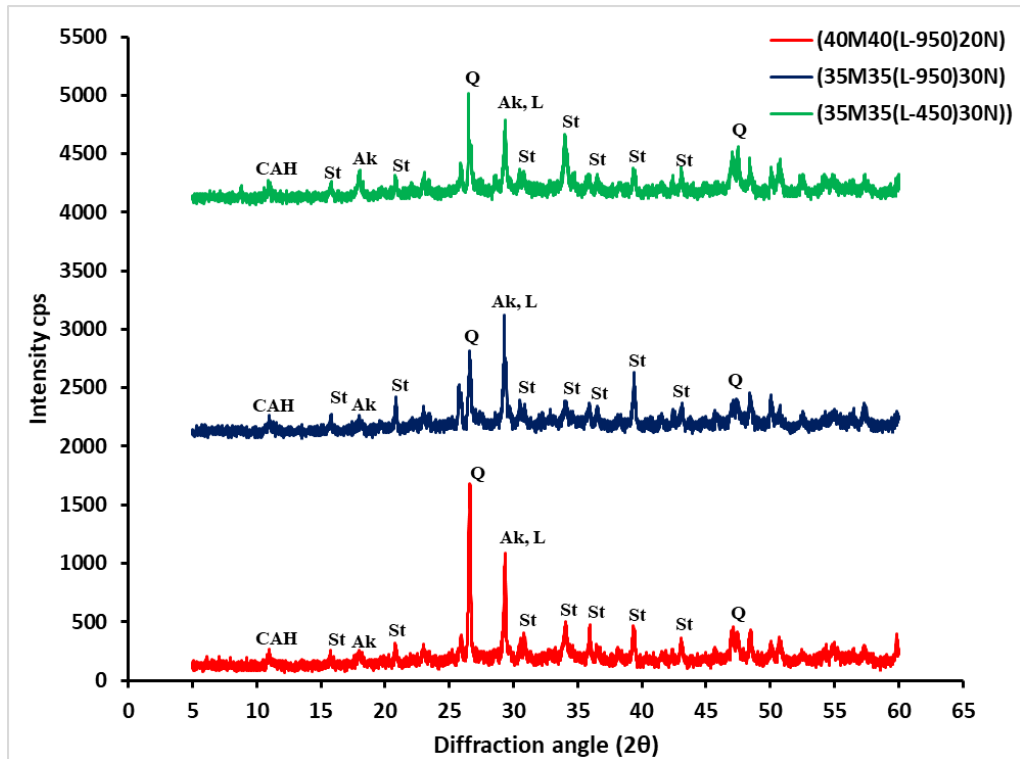
435

436

437

### 438 3.4 Reaction hydrates analysis by XRD

439 X-Ray diffraction (XRD) analysis, was investigated for pastes of samples with the highest strength  
440 (40M40(L-950)20N, (35M35(L-950)30N) and (35M35(L-450)30N)) at age of 28 days, as  
441 presented in Figure. 13. Major hydration products can be identified and are composed chiefly of  
442 CaO-Al<sub>2</sub>O<sub>3</sub>-MgO-SiO<sub>2</sub> compounds. The utilisation of a dry alkaline (CaO) activator in the mix  
443 transforms the crystallinity diffraction patterns into amorphicity status and leads to the presence  
444 of prevailing vitreous phases. The major hydrated phases were specifically, tetra calcium  
445 aluminate hydrate; CAH (C<sub>4</sub>AH<sub>13</sub>); calcium aluminum silicate hydrates; St (stratlingite –  
446 C<sub>2</sub>ASH<sub>8</sub>); and Akermanite; Ak (Ca<sub>2</sub>MgSi<sub>2</sub>O<sub>7</sub>) (Kim *et al.*, 2013)(Gameiro *et al.*, 2014)(Gameiro  
447 *et al.*, 2012)(Gameiro *et al.*, 2011). Moreover, Gameiro (Gameiro *et al.*, 2012) stated that calcium  
448 silicate hydrate (CSH) is viewed to overlap with the lime (calcite) peak in these blends, with higher  
449 MK ( $\geq 33\%$  MK). XRD patterns of (40M40(L-950)20N) reveals a gentle reduction of the dominant  
450 Quartz (SiO<sub>2</sub>) crystalline phase that existed in the raw MK in the range of  $2\theta = 26^\circ$ . This slight  
451 reduction indicates two facts; firstly, the remaining large amounts of this crystalline quartz are in  
452 a non-reactant status, secondly, low CaO amounts, which were less than that what was required,  
453 in order to dissolve this phase, which in terms led to less strength. However, a glassy phase of  
454 alumina-silicate gel (C-A-S-H) can be indicated in the range  $2\theta 25^\circ$ - $30^\circ$  due to the semi-  
455 amorphous nature (Escalante-García *et al.*, 2003; Elimbi *et al.*, 2014). At the same time, the strong  
456 presence of stratlingite is noticed as a permanent phase in the matrix. The formulation of  
457 stratlingite as dominant peaks in the three blends indicates that this hydrate is stable and is verified  
458 as the hydrate responsible for the enhancement of mechanical strength (Bakolas *et al.*, 2006;  
459 Gameiro *et al.*, 2012). As would be expected, crystalline quartz has decreased in (35M35(L-  
460 950)30N), as the amount of LKD was increased to 30%. The growth of stratlingite peaks can be  
461 noticed clearly through the entire range of diffraction with the increment of LKD causing higher  
462 strength for the blend. This indicates that the lime (CaO) generated from LKD has caused  
463 significant dissolution of aluminate and silicate species (Morsy *et al.*, 2017). The high amounts of  
464 MgO from NP has strongly contributed to presence of amorphous phases, such as Akermanite  
465 together with the reactive CaO from LKD. This reaction introduced new bonds such as Ca-Mg-Si,  
466 which have high contribution to the strength. C<sub>4</sub>AH<sub>13</sub> was present in minor quantities due to the  
467 instability of this phase through the curing aging (Gameiro *et al.*, 2012). Additionally, portlandite  
468 (Ca(OH)<sub>2</sub>) peaks were not found extensively due to the modified LKD and MK in the blends, as  
469 this peak may appear in low MK blends (Gameiro *et al.*, 2012). A range of reaction products can  
470 be noticed similarly in (35M35(L-450)30N) with LKD calcined at 450°C, indicating that  
471 comparative diffractions were formulated for this blend with (35M35(L-950)30N) and LKD  
472 calcined at 950°C. This was observed in the strength development for both levels of thermal  
473 treatment.



474

475 *Figure 13. XRD patterns of (40M40(L-950)20N), (35M35(L-950)30N) and (35M35(L-450)30N) at age of 28 days.*

476

### 477 3.5 Molecular identification of hydrates by FT-IR

478 The FTIR spectra was reproduced for pastes with the highest compressive strength and were  
 479 investigated after 28 days of curing, as shown in Figure. 14. In all spectra, the C-O band ranging  
 480 from 1413, 1416 and 1417 and 874, 875 and 873  $\text{cm}^{-1}$  were observed, and similar to infrared in the  
 481 raw LKD in Figure. 14. The wide stretching band starting from 1200-900  $\text{cm}^{-1}$  region of Si-O and  
 482 Al-O were noticed in all the spectra of the blends. These bands reveal the strong evidence of  
 483 Aft/AFm phases such as Stratlingite ( $\text{C}_2\text{ASH}_8$ ) and Mono-Carboaluminate  $\text{Ca}_4\text{Al}_2(\text{CO}_3)(\text{OH})_{12} /$   
 484  $5\text{H}_2\text{O}$  (Horgnies *et al.*, 2013). A smooth shifting of Si-O and Al-O can be detected for (35M35(L-  
 485 450)30N), proving that treatment at 450°C for LKD has contributed significantly in formulating  
 486 similar bands compared to treatment at 950°C.

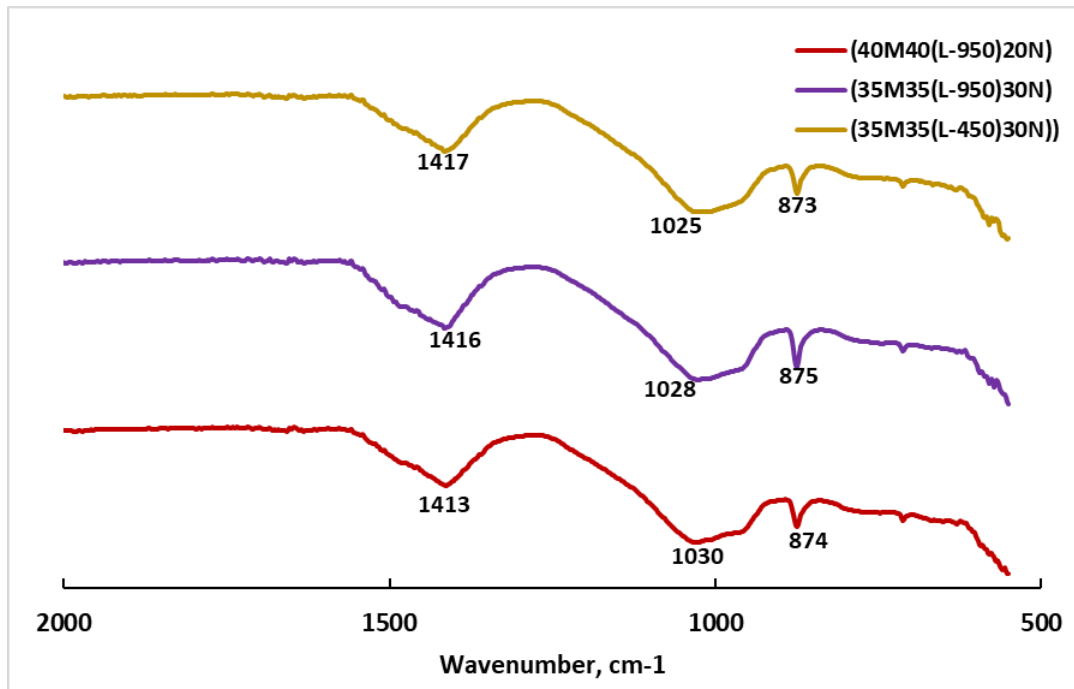


Figure 14. FTIR-spectra of hardened pastes at age of 28 days curing.

487

488

489

### 490 3.6 Microstructure and EDX analysis

491 The SEM micrographs for (40M40(L-950)20N), (35M35(L-950)30N) and (35M35(L-450)30N) at  
 492 age of 28 days of curing are shown in Figure. 15. The microstructure of hardened pastes shows the  
 493 prevalence of stratlingite ( $C_2ASH_8$ ) with dense-like microstructure (Gameiroa *et al.*, 2011). The  
 494 strong occurrence of  $C_2ASH_8$  has specified by the appearance of rodlets of AFt phases. This  
 495 illustrates the pozzolanic reaction of Si and Al with  $Ca^{+2}$  cations, which encourages further  
 496 dissolution and breaking the Si–O and Al–O bonds in both MK and NP (Medina *et al.*, 2016).  
 497 EDX values have showed that major chemical elements include O, Al, Si and Ca; as shown in  
 498 Table 5; which represent key elements responsible for the strength of blends. Moreover, minor  
 499 elements were noticed such as K, Ti ,Fe and S. The Ca/Si ratio in C-A-S-H phase are similar in  
 500 both (40M40(L-950)20N) and (35M35(L-950)30N) with 0.97 and 1.03 which indicates increased  
 501 reaction of both elements and formation of hydrate products in the form of (stratlingite –  
 502  $C_2ASH_8$ )(Abdel-Gawwad *et al.*, 2019). On the opposite, Ca/Si ratio of (35M35(L-450)30N) was  
 503 very high (2.71) which indicates less reaction of ( $Ca^{+2}$ ).

504

505

506

507

508



509

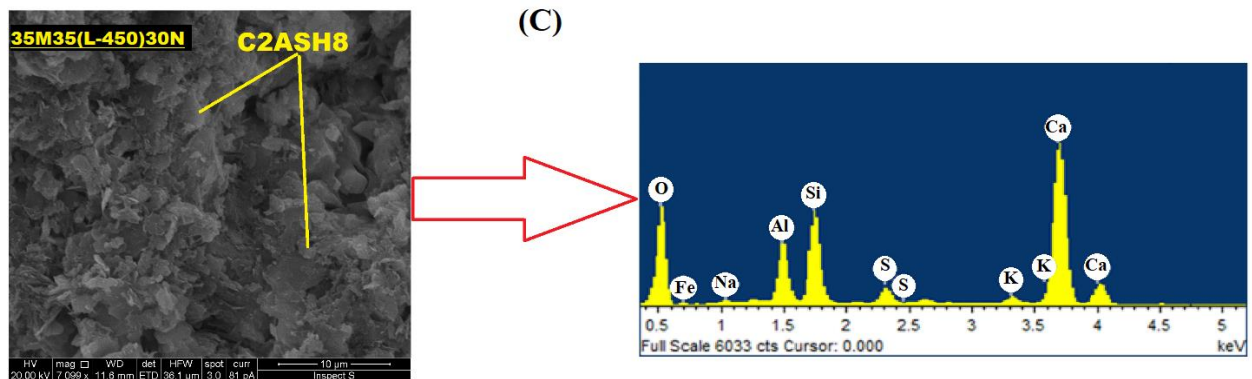
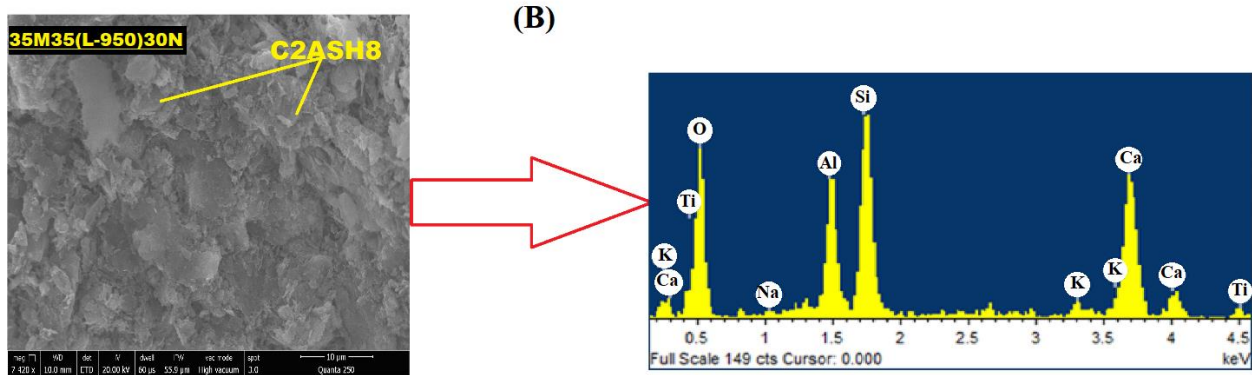
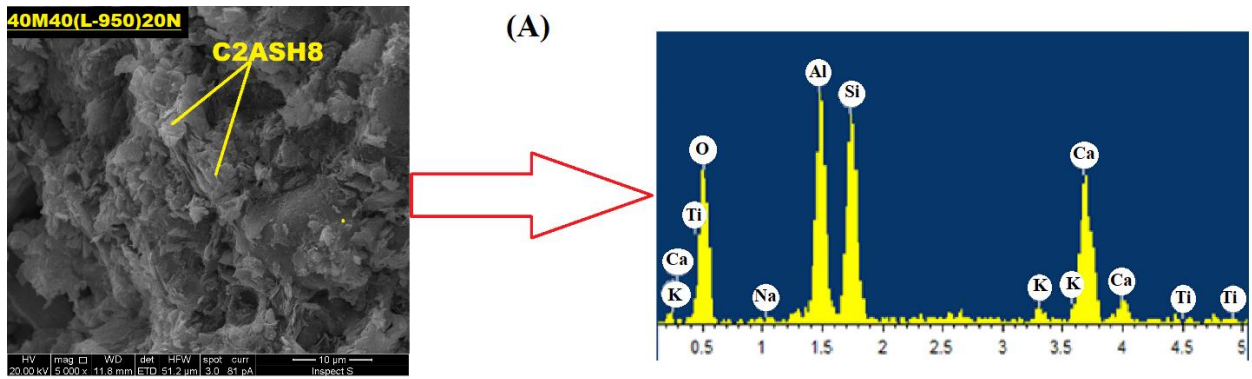
Table 5. Elemental composition measured by SEM/EDX

510

*for (40M40(L-950)20N) , (35M35(L-950)30N), (35M35(L-450)30N) at age of 28 days.*

Element(wt. %)	Mixtures		
	Spectrum of (40M40(L-950)20N	Spectrum of (35M35(L- 950)30N)	Spectrum of (35M35(L- 450)30N)
<b>O</b>	58.46	61.22	57.8
<b>Si</b>	13.95	13.95	8.94
<b>Al</b>	12.87	8.07	5.54
<b>Ca</b>	13.56	14.4	24.25
<b>Ti</b>	1.17	1.33	0
<b>K</b>	0	1.03	0.81
<b>S</b>	0	0	1.74
<b>Fe</b>	0	0	0.48

511



512

513

514

515

516

Figure 15. SEM micrographs and EDX analysis for 40M40(L-950)20N, (35M35(L-950)30N) and (35M35(L-450)30N) at age of 28 days.

517 **4. Conclusions**

518 The research investigated the use of a waste material (Lime Kiln Dust) as a potential source of  
519 earth alkaline (CaO), for activating a combination of alumina-silicate materials to formulate one-  
520 part AAC. An assisted activation approach achieved by thermal treatment at two different  
521 temperatures (950°C and 450°C), was used for increasing the reactivity of materials. Comparisons  
522 were made between the performance of raw materials and thermal treatment as well as between  
523 different chosen blends by using techniques of analysis including compressive strength, XRD, TG-  
524 DTA, FTIR and SEM/EDX. The experimental investigations gave the following conclusions:

- 525 • The highest compressive strength that, was recorded is 27.3MPa at age of 28 days for mortar  
526 comprising treated LKD at 950 °C. Comparative compressive strength was gained at 450°C  
527 calcination level, indicating that the reactivity of materials started to increase at this  
528 temperature. The development of strength was attributed to the progressive pozzolanic reaction  
529 during the curing period.
- 530 • Thermal treatment was evidently participating in breaking the crystalline phases of the original  
531 materials and strong evidence of transformation to amorphous phases was provided by XRD,  
532 TG-DTA and FTIR results. Remarkably, this was noticed significantly at 450°C, which saved  
533 a considerable amount of energy.
- 534 • Synthesised products characterised by XRD, FTIR and SEM/EDX methods revealed that the  
535 formation of the prevalence of hydrates responsible for the strength. These products include  
536 chiefly stratlingite (C<sub>2</sub>ASH<sub>8</sub>) and Akermanite; Ak (Ca<sub>2</sub>MgSi<sub>2</sub>O<sub>7</sub>). XRD spectra proved that with  
537 the increment of LKD in mix, came increments of strength products formulation.
- 538 • The findings of the study, has proved that lime waste (LKD) has a high potential to be a solid  
539 alkaline activator if treated properly and its impurities are removed.

541 **Acknowledgement**

542 The first author would like to acknowledge the financial support provided by the Iraqi Ministry of  
543 Higher Education and Scientific Research and the University of Babylon.

544

545

546

547

548

549

## 550 References

- 551 Abdel-Gawwad, H. A., García, S. R. V. and Hassan, H. S. (2018) ‘Thermal activation of air cooled  
552 slag to create one-part alkali activated cement’, *Ceramics International*, 44(12), pp. 14935–14939.
- 553 Abdel-Gawwad, H. A. and Khalil, K. A. (2018) ‘Application of thermal treatment on cement kiln  
554 dust and feldspar to create one-part geopolymer cement’, *Construction and Building Materials*,  
555 187, pp. 231–237.
- 556 Abdel-Gawwad, H. A., Rashad, A. M. and Heikal, M. (2019) ‘Sustainable utilization of pretreated  
557 concrete waste in the production of one-part alkali-activated cement’, *Journal of Cleaner*  
558 *Production*. Elsevier, 232, pp. 318–328.
- 559 Almalkawi, A. T., Hamadna, S. and Soroushian, P. (2017) ‘One-part alkali activated cement based  
560 volcanic pumice’, *Construction and Building Materials*, 152, pp. 367–374.
- 561 Bakolas, A. *et al.* (2006) ‘Evaluation of pozzolanic activity and physico-mechanical characteristics  
562 in metakaolin-lime pastes’, *Journal of Thermal Analysis and Calorimetry*, 84(1), pp. 157–163.
- 563 Ban, C. C., Ken, P. W. and Ramli, M. (2017) ‘Mechanical and Durability Performance of Novel  
564 Self-activating Geopolymer Mortars’, *Procedia Engineering*, 171(Supplement C), pp. 564–571.
- 565 British Standard Institution (BSI) (2010) *196-6: 2010, Methods of testing cement, Determination*  
566 *of fineness*, London, England: British Standard Institution (BSI). London: BSI Standards Limited.
- 567 British Standard Institution (BSI) (2016) *196-1: 2016, Methods of Testing Cement, Determination*  
568 *of Strength*, London, England: British Standard Institution (BSI). London: BSI Standards Limited.
- 569 Cabrera, J. and Rojas, M. F. (2001) ‘Mechanism of hydration of the metakaolin–lime–water  
570 system’, *Cement and Concrete Research*. Elsevier, 31(2), pp. 177–182.
- 571 Davidovits, J. (1993) ‘Geopolymer cements to minimise carbon-dioxide greenhouse-warming’,  
572 *Ceram. Trans.*, 37, pp. 165–182.
- 573 Davidovits, J. (2017) ‘Geopolymers based on natural and synthetic metakaolin-A critical review’,  
574 *on Advanced Ceramics and Composites*. Wiley Online Library, 38(3), p. 201.
- 575 Demie, S., Nuruddin, M. F. and Shafiq, N. (2013) ‘Effects of micro-structure characteristics of  
576 interfacial transition zone on the compressive strength of self-compacting geopolymer concrete’,  
577 *Construction and Building Materials*, 41, pp. 91–98.
- 578 Van Deventer, J. S. J., Provis, J. L. and Duxson, P. (2012) ‘Technical and commercial progress in  
579 the adoption of geopolymer cement’, *Minerals Engineering*, 29(Supplement C), pp. 89–104.
- 580 Duxson, P., Lukey, G. C. and van Deventer, J. S. J. (2007) ‘Physical evolution of Na-geopolymer  
581 derived from metakaolin up to 1000 C’, *Journal of Materials Science*. Springer, 42(9), pp. 3044–  
582 3054.
- 583 Eilers, L. H., Nelson, E. B. and Moran, L. K. (1983) ‘High-temperature cement compositions-  
584 pectolite, scawtite, truscottite, or xonotlite: which do you want?’, *Journal of Petroleum*  
585 *Technology*. Society of Petroleum Engineers, 35(07), pp. 1–373.
- 586 Elimbi, A. *et al.* (2014) ‘Thermal behavior and characteristics of fired geopolymers produced from  
587 local Cameroonian metakaolin’, *Ceramics International*. Elsevier, 40(3), pp. 4515–4520.

- 588 Escalante-García, J. I. *et al.* (2003) ‘Hydration Products and Reactivity of Blast-Furnace Slag  
589 Activated by Various Alkalis’, *Journal of the American Ceramic Society*. Wiley Online Library,  
590 86(12), pp. 2148–2153.
- 591 Feng, D., Provis, J. L. and van Deventer, J. S. J. (2012) ‘Thermal Activation of Albite for the  
592 Synthesis of One-Part Mix Geopolymers’, *Journal of the American Ceramic Society*. John Wiley  
593 & Sons, Ltd (10.1111), 95(2), pp. 565–572.
- 594 Gameiro, A. *et al.* (2012) ‘Hydration products of lime–metakaolin pastes at ambient temperature  
595 with ageing’, *Thermochimica Acta*, 535, pp. 36–41.
- 596 Gameiro, A. *et al.* (2014) ‘Physical and chemical assessment of lime–metakaolin mortars:  
597 Influence of binder:aggregate ratio’, *Cement and Concrete Composites*, 45, pp. 264–271.
- 598 Gameiro, A. *et al.* (2011) ‘Metakaolin-Lime Hydration Products and Phase Stability: A  
599 Microscopy Analysis’, *BOOK OF EXTENDED*, p. 31.
- 600 Garbev, K. *et al.* (2008) ‘First Observation of  $\alpha$ -Ca<sub>2</sub> [SiO<sub>3</sub> (OH)](OH)–Ca<sub>6</sub> [Si<sub>2</sub>O<sub>7</sub>][SiO<sub>4</sub>](OH)  
601 2 Phase Transformation upon Thermal Treatment in Air’, *Journal of the American Ceramic  
602 Society*. Wiley Online Library, 91(1), pp. 263–271.
- 603 He, P. *et al.* (2010) ‘Effect of cesium substitution on the thermal evolution and ceramics formation  
604 of potassium-based geopolymer’, *Ceramics International*. Elsevier, 36(8), pp. 2395–2400.
- 605 Heath, A. *et al.* (2013) ‘The potential for using geopolymer concrete in the UK’, *Proceedings of  
606 the Institution of Civil Engineers: Construction Materials*, 166(4), pp. 195–203.
- 607 Hill, J. O. and Verma, R. K. (2019) ‘Thermal Analysis | Coupled Techniques☆’, in Worsfold, P.  
608 *et al.* (eds). Oxford: Academic Press, pp. 6–11.
- 609 Horgnies, M., Chen, J. J. and Bouillon, C. (2013) ‘Overview about the use of Fourier Transform  
610 Infrared spectroscopy to study cementitious materials’, *WIT Transactions on Engineering  
611 Sciences*, 77, pp. 1743–3533.
- 612 Ilić, B. R., Mitrović, A. A. and Miličić, L. R. (2010) ‘Thermal treatment of kaolin clay to obtain  
613 metakaolin’, *Hemijaska industrija*, 64(4), pp. 351–356.
- 614 Justnes, H. *et al.* (1990) ‘Nuclear magnetic resonance (NMR)—a powerful tool in cement and  
615 concrete research’, *Advances in Cement Research*. Thomas Telford Ltd, 3(11), pp. 105–110.
- 616 Kakali, G. *et al.* (2001) ‘Thermal treatment of kaolin: the effect of mineralogy on the pozzolanic  
617 activity’, *Applied Clay Science*, 20(1), pp. 73–80.
- 618 Kim, M. S. *et al.* (2013) ‘Use of CaO as an activator for producing a price-competitive non-cement  
619 structural binder using ground granulated blast furnace slag’, *Cement and Concrete Research*, 54,  
620 pp. 208–214.
- 621 Kimata, M. *et al.* (1996) ‘Anorthite megacrysts from island arc basalts’, *Oceanographic Literature  
622 Review*, 1(43), p. 50.
- 623 Li, C., Sun, H. and Li, L. (2010) ‘A review: The comparison between alkali-activated slag (Si+  
624 Ca) and metakaolin (Si+ Al) cements’, *Cement and Concrete Research*. Elsevier, 40(9), pp. 1341–  
625 1349.
- 626 Li, X., Wang, Z. and Jiao, Z. (2013) ‘Influence of curing on the strength development of calcium-

627 containing geopolymer mortar’, *Materials*. School of Civil Engineering, Harbin Institute of  
628 Technology, Harbin 150006, China, 6(11), pp. 5069–5076.

629 Licht, S. (2016) ‘Process for synthesis of calcium oxide’.

630 Luukkonen, T. *et al.* (2018) ‘One-part alkali-activated materials: A review’, *Cement and Concrete*  
631 *Research*. Elsevier, 103, pp. 21–34.

632 Matakah, F. *et al.* (2016) ‘Mechanochemical synthesis of one-part alkali aluminosilicate hydraulic  
633 cement’, *Materials and Structures*, 50(1), p. 97.

634 Medina, C. *et al.* (2016) ‘Mineralogy and microstructure of hydrated phases during the pozzolanic  
635 reaction in the sanitary ware waste/Ca (OH) 2 system’, *Journal of the American Ceramic Society*.  
636 Wiley Online Library, 99(1), pp. 340–348.

637 Miguel, G.-R. *et al.* (2009) ‘Characterization of Calcium Carbonate, Calcium Oxide, and Calcium  
638 Hydroxide as Starting Point to the Improvement of Lime for Their Use in Construction’, *Journal*  
639 *of Materials in Civil Engineering*. American Society of Civil Engineers, 21(11), pp. 694–698.

640 Miller, M. M. and Callaghan, R. M. (2004) ‘Lime Kiln Dust as a Potential Raw Material in  
641 Portland Cement Manufacturing’.

642 Mineralproducts.org (2017) ‘Novel cements: low energy, low carbon cements’.  
643 Mineralproducts.org.

644 Morsy, M. S. *et al.* (2017) ‘Mechanical properties, phase composition and microstructure of  
645 activated Metakaolin-slaked lime binder’, *KSCCE Journal of Civil Engineering*. Springer, 21(3),  
646 pp. 863–871.

647 Nath, P. and Sarker, P. K. (2015) ‘Use of OPC to improve setting and early strength properties of  
648 low calcium fly ash geopolymer concrete cured at room temperature’, *Cement and Concrete*  
649 *Composites*. Elsevier, 55, pp. 205–214.

650 Nayak, P. S. and Singh, B. K. (2007) ‘Instrumental characterization of clay by XRF, XRD and  
651 FTIR’, *Bulletin of Materials Science*. Springer, 30(3), pp. 235–238.

652 Peng, M. X. *et al.* (2017) ‘Effects of alkali on one-part alkali-activated cement synthesized by  
653 calcining bentonite with dolomite and Na<sub>2</sub>CO<sub>3</sub>’, *Applied Clay Science*. School of Materials  
654 Science and Engineering, Hunan University of Science and Technology, Xiangtan, China, 139,  
655 pp. 64–71.

656 Perera, D. S. *et al.* (2007) ‘Influence of curing schedule on the integrity of geopolymers’, *Journal*  
657 *of materials science*. Springer, 42(9), pp. 3099–3106.

658 ‘Production of purified calcium carbonate’ (1993).

659 Provis, J. L. (2014) ‘Introduction and scope’, *RILEM State-of-the-Art Reports*. Department of  
660 Materials Science and Engineering, University of Sheffield, Sheffield, United Kingdom, pp. 1–9.

661 Provis, J. L. (2017) ‘Alkali-activated materials’, *Cement and Concrete Research*.

662 Provis, J. L. and Bernal, S. A. (2014) ‘Geopolymers and related alkali-activated materials’, *Annual*  
663 *Review of Materials Research*. Annual Reviews, 44, pp. 299–327.

664 Provis, J. L., Palomo, A. and Shi, C. (2015) ‘Advances in understanding alkali-activated  
665 materials’, *Cement and Concrete Research*, 78.

666 Ramachandran, V. S. and Beaudoin, J. J. (2000) *Handbook of analytical techniques in concrete*  
667 *science and technology: principles, techniques and applications*. Elsevier.

668 Rashad, A. M. (2013) ‘Metakaolin as cementitious material: History, scours, production and  
669 composition – A comprehensive overview’, *Construction and Building Materials*, 41, pp. 303–  
670 318.

671 Rashad, A. M., Hassan, A. A. and Zeedan, S. R. (2016) ‘An investigation on alkali-activated  
672 Egyptian metakaolin pastes blended with quartz powder subjected to elevated temperatures’,  
673 *Applied Clay Science*, 132–133, pp. 366–376.

674 Sanz, J. *et al.* (1988) ‘Aluminum-27 and Silicon-29 magic-angle spinning nuclear magnetic  
675 resonance study of the kaolinite-mullite transformation’, *Journal of the American Ceramic Society*.  
676 Wiley Online Library, 71(10), pp. C418–C421.

677 Singh, B. *et al.* (2015) ‘Geopolymer concrete: A review of some recent developments’,  
678 *Construction and building materials*. Elsevier, 85, pp. 78–90.

679 Torres-Carrasco, M. and Puertas, F. (2017) ‘Alkaline activation of different aluminosilicates as an  
680 alternative to Portland cement: alkali activated cements or geopolymers’, *Revista Ingeniería de*  
681 *Construcción*, 32(2), pp. 5–12.

682 U.S. Geological Survey (2019) *Mineral commodity summaries 2019*. Virginia.

683 Vaccari, M., Gialdini, F. and Collivignarelli, C. (2013) ‘Study of the reuse of treated wastewater  
684 on waste container washing vehicles’, *Waste management*. Elsevier, 33(2), pp. 262–267.

685 Vizcayno, C. *et al.* (2010) ‘Pozzolan obtained by mechanochemical and thermal treatments of  
686 kaolin’, *Applied Clay Science*. Elsevier, 49(4), pp. 405–413.

687 Weerdt, K. De (2011) *Geopolymers – State of the art*. Blindern.

688 Yao, X. *et al.* (2009) ‘Geopolymerization process of alkali–metakaolinite characterized by  
689 isothermal calorimetry’, *Thermochimica Acta*. Elsevier, 493(1–2), pp. 49–54.

690

691

692

693

694

695

696

697

698

699

700

701 **List of Figures**

702 Figure 1. Particle size distribution (PSD) of starting materials. .... 5  
703 Figure 2. XRD-patterns of initial materials ..... 8  
704 Figure 3. SEM micrographs of a) MK, b) LKD and c) NP. .... 9  
705 Figure 4. FTIR-spectra of Raw MK, NP and LKD..... 10  
706 Figure 5. TG-DTA curves of A: NP, B: MK, C: LKD ..... 11  
707 Figure 6. Preparation steps of one-part (AAC)..... 13  
708 Figure 7 Particle Size Distribution of the used sand..... 13  
709 Figure 8. Compressive strength of initial mixes ..... 14  
710 Figure 9. XRD patterns of materials after thermal treatment A)MK, B)NP, C)LKD. .... 17  
711 Figure 10. FTIR spectra of materials after thermal treatment. .... 18  
712 Figure 11. Compressive strength after 950 °C calcination. .... 19  
713 Figure 12. Compressive strength after 450°C calcination ..... 20  
714 Figure 13. XRD patterns of (40M40(L-950)20N),(35M35(L-950)30N) and (35M35(L-450)30N))  
715 at age of 28 days. .... 22  
716 Figure 14. FTIR-spectra of hardened pastes at age of 28 days curing..... 23  
717 Figure 15. SEM micrographs and EDX analysis ..... 25  
718

719 **List of Tables**

720 Table 1. Physical properties of undisturbed materials. .... 4  
721 Table 2. Chemical composition by XRF of raw materials (Wt.%)..... 5  
722 Table 3. Initial mixes proportion ..... 14  
723 Table 4. Mixing proportions of blends. .... 15  
724 Table 5. Elemental composition measured by SEM/EDX..... 24  
725